Journal of Hazardous Materials 470 (2024) 134185

Contents lists available at ScienceDirect

Journal of Hazardous Materials

journal homepage: www.elsevier.com/locate/jhazmat

Adsorption of PFAS onto secondary microplastics: A mechanistic study

Omobayo A. Salawu [a,b], Christopher I. Olivares [a,b], Adeyemi S. Adeleye [a,b,c,*]

[a] Department of Civil and Environmental Engineering, University of California, Irvine, CA 92697-2175, USA
[b] The Water-Energy Nexus Centre, University of California, Irvine, CA 92697-2175, USA
[c] Department of Earth and Environmental Engineering, Columbia University, New York, NY 10027-6623, United States

HIGHLIGHTS

- PET microplastics (MPs) were produced from PET water bottles.
- The adsorption of PFAS to the MPs was thermodynamically spontaneous at 25 °C.
- ΔS and change in the intensity of the IR peak at 1089 cm^{-1} significantly correlated.
- The q_e of MPs for PFAS increased as ionic strength or temperature increased.
- The q_e of MPs for PFAS decreased as pH or NOM concentration increased.

GRAPHICAL ABSTRACT

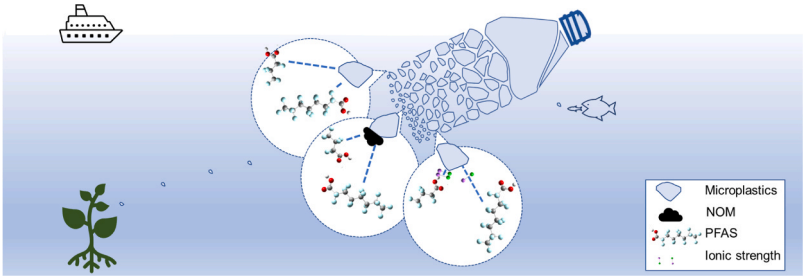

ARTICLE INFO

Keywords:
Forever chemicals
Fluorochemicals
Plastics
Water chemistry

ABSTRACT

Microplastics (MPs) are abundant in aquatic systems. The ecological risks of MPs may arise from their physical features, chemical properties, and/or their ability to concentrate and transport other contaminants, such as per- and polyfluoroalkyl substances (PFAS). PFAS have been extracted from MPs found in natural waters. Still, there needs to be a mechanistic investigation of the effect of PFAS chemistry and water physicochemical properties on how PFAS partition onto secondary MPs. Here, we studied the influence of pH, natural organic matter (NOM), ionic strength, and temperature on the adsorption of PFAS on MPs generated from PET water bottles. The adsorption of PFAS to the MPs was thermodynamically spontaneous at 25 °C, based on Gibb's free energy ($\Delta G = -16$ to -23 kJ/mol), primarily due to increased entropy after adsorption. Adsorption reached equilibrium within 7–9 h. Hence, PFAS will partition to the surface of secondary PET MPs within hours in fresh and saline waters. Natural organic matter decreased the capacity of secondary PET MPs for PFAS through electrosteric repulsion, while higher ionic strength favored PFAS adsorption by decreasing electrostatic repulsion. Increased pH increased electrostatic repulsion, which negated PFAS adsorption. The study provides fundamental information for developing models to predict interactions between secondary MPs and PFAS.

1. Introduction

Due to their lightweight, durability, and cost-effectiveness, plastics are widely used in various domestic and industrial applications, leading to a skyrocketing production rate [1,2]. About 391 million tons of plastics were produced in 2021, and production is estimated to double in 20 years [1,3,4]. High global plastic production and use have led to increasing amounts of plastic wastes in the environment [5–8], where

* Corresponding author at: Department of Civil and Environmental Engineering, University of California, Irvine, CA 92697-2175, USA.
E-mail address: asa2296@columbia.edu (A.S. Adeleye).

https://doi.org/10.1016/j.jhazmat.2024.134185
Received 14 January 2024; Received in revised form 29 March 2024; Accepted 30 March 2024
Available online 31 March 2024

they may be subjected to fragmentation due to mechanical, chemical, and biological processes [9,10]. Plastics (and their debris) may occur as macroplastics (size > 25 mm), mesoplastics (5–25 mm), microplastics (1 μm–5 mm), and nanoplastics (1–1000 nm) [8,11,12]. Microplastics (MPs) are a significant global challenge in aquatic and terrestrial environments [13,14]. The ecological risks of MPs may arise from their physical properties (e.g., sharp edges), chemical properties (e.g., leaching of additives) [8,15–17], and/or their ability to concentrate and transport other contaminants [2,18].

MPs tend to adsorb various legacy and emerging contaminants, including per- and polyfluoroalkyl substances (PFAS) [2,19]. PFAS are currently one of the most important emerging contaminants due to their ubiquity, persistence, toxicity, and bioaccumulation in organisms [20–23]. Cheng and coworkers detected up to 9 μg/g total PFAS on MPs isolated from an urban river [7]. The authors reported that perfluorooctane sulfonic acid (PFOS) and perfluorooctanoic acid (PFOA) were the most abundant PFAS adsorbed to the MPs [7,24]. The occurrence of PFAS on MPs suggests that MPs may transport PFAS into organisms. In fact, PFAS and MPs were recently detected in the guts of organisms on the Mississippi coast, which may confirm the suggestion. MPs can be intentionally engineered to be small (primary MPs) or may form from the fragmentation of larger plastics (secondary MPs) [25–28]. Although secondary MPs are more abundant than primary MPs in aquatic systems [14], most existing studies of partitioning of PFAS onto MPs were performed using primary MPs. The physicochemical properties of secondary MPs, such as their shape, surface roughness, composition, functionality, and affinity, may differ from those of primary MPs, and lead to changes in their ability to convey PFAS in water [8,19,27,29,30].

Ateia et al. found more PFAS partitioned (per unit surface area) to the surface of secondary MPs than their primary counterparts [27]. The higher PFAS uptake by the secondary MPs was attributed to surface roughness and/or the presence of additives [27]. To date, however, there is no mechanistic investigation of the effect of PFAS chemistry or water chemistry on how PFAS partition onto secondary MPs. A preliminary study that we conducted revealed that the adsorption capacity of secondary polyethylene terephthalate (PET) MPs for five PFAS (comprising of carboxylates and sulfonates) was 21.6–243.9 % higher than that of the primary counterpart. More interestingly, while the rate constants for the adsorption of the carboxylates were lower for the secondary PET MPs (compared to the primary PET MPs), they were higher for the secondary PET MPs when the PFAS had sulfonated head groups (Fig. S1). Therefore, adsorption parameters determined with primary MPs may not accurately predict those of secondary MPs, even if they share the same material chemistry.

Although hydrophobic interaction is essential in the partitioning of PFAS onto surfaces [27,31,32], other interaction forces that may be sensitive to aqueous chemistry, such as electrostatic interactions, may play important roles in PFAS partitioning onto secondary MPs [31,33]. The main objectives of this study were to investigate the role of water physicochemical properties (pH, ionic strength, natural organic matter [NOM], and temperature) and PFAS chemistry (chain length and functional group) on PFAS partitioning from water to the surface of secondary MPs. PET was selected for this study because it is the second most-produced thermoplastic, with a market of 53 million tonnes in 2010 [34]. The most produced thermoplastic, polyethylene (with a market value of 73 million tonnes in 2010), has been more widely studied. This study is based on a central hypothesis that the extent to which water chemistry influences PFAS partitioning onto the surface of secondary MPs is a function of PFAS chain length.

2. Materials and methods

2.1. Production of secondary MPs from PET bottles

We produced the secondary PET MPs used in this study by modifying a method described by Ji and co-workers [35]. Briefly, we cut PET bottles to card sizes. We then shredded the card-size plastics to 0.5 × 4.0 cm with a paper shredder. We further cut the plastics into smaller pieces (~ 0.5 × 1.0 cm), and mechanically degraded them with a hand blender (Yissvic LB2108, Ningbo, China) for a total blending time of 240 min in a glass beaker that contains 0.05 % Bovine Serum Albumin (BSA, ≥99.0 %, Fisher BioReagents, Fair Lawn, NJ) prepared in deionized (DI) water (18.2 MΩ cm, Milli-Q Ultrapure Water Systems). We used the BSA to prevent MPs agglomeration during blending [35,36]. Blenders were used for 30 s at a time and allowed to cool down for 5 min afterward. After blending, we sieved the MPs suspensions with stacked sieves (Hogentogler, Gerwig Lane, DC) to isolate MPs within 53 – 250 μm, which falls within the MPs size range observed in different aquatic media [37–39]. To remove BSA from the surface of the MPs, we dialyzed the sieved MPs against DI water for 5 d using Spectra/Por 3 RC dialysis membrane (3500 Da) and confirmed complete removal via UV–vis spectrophotometry and Fourier-transformed infrared (FTIR) spectroscopy. Following dialysis, we dried the MPs in an oven at 50ºC for 12 h and stored them until use.

2.2. Characterization of secondary PET MPs

We determined the morphology of the secondary MPs using a FEI Magellan 400 scanning electron microscope (SEM; FEI, USA). Their size distribution, representing the MPs' lateral dimension, was obtained using light microscopy and ImageJ analysis. Size was determined by measuring the distance from one edge to another at six different positions across each particle, and the average value was reported. We used FTIR spectroscopy to characterize the functional groups on the surface of the MPs (and compared them with that of the original PET bottle) using a Jasco FT/IR-4700 spectrometer (Japan). Following established methods [40,41], we determined the surface charge of the MPs by measuring their zeta (ζ) potential using a NanoBrook 90Plus (Brookhaven Instruments, Holtsville, NY). We also characterized the MPs' Brunauer-Emmett-Teller (BET) surface area through nitrogen sorption using a Micromeritics 3Flex Surface Characterization Analyzer (Norcross, GA).

2.3. PFAS adsorption studies

We studied the adsorption of PFAS onto the secondary PET MPs by batch experiments. We considered five PFAS for this study, including PFOS, PFOA, perfluorobutanoic acid (PFBA), hexafluoropropylene oxide dimer acid (GenX), and perfluorobutane sulfonic acid (PFBS). More details of the PFAS and their physicochemical properties are provided in Table S1. The preparation of PFAS stock and solution is described in Section S1 of the Supplementary Document. For the batch studies, we added 20 mg of PET MPs to 10 mL of each aqueous PFAS solution (200 μg/L) in 15 mL polystyrene tubes. Although the PFAS concentration we used is higher than what is typically detected in natural waters and wastewater (which is in the ng/L range) [42,43], our previous study revealed that it is nearly impractical to perform PFAS adsorption studies at ng/L levels and obtain the 10–85 % adsorbate removal recommended by the ASTM for batch studies [44], due to PFAS adsorption to containers [32]. We, in fact, selected polystyrene tubes based on our previous study, which shows low adsorption of the selected PFAS to the container material [32]. We performed all the experiments in triplicates with triplicate controls (PFAS solutions with no MPs, to quantify partitioning to the container). We quantified the equilibrium PFAS concentrations via liquid chromatography with tandem mass spectrometry (LC-MS/MS) using an Agilent 6470 LC/TQ (Santa Clara, CA). We provided detailed information on equilibrium PFAS concentration determination and LC-MS/MS analysis in Section S2. We also performed adsorption kinetics studies to determine the equilibrium adsorption time and maximum adsorption capacity of the MPs for (1) each PFAS (200 μg/L) and (2) a mixture of the five PFAS (each PFAS in the mixture =

200 μg/L). To understand the effect of water chemistry on the adsorption of PFAS to the MPs, we varied pH (3–11), ionic strength (0–100 mM Na^+), and NOM concentration (0–100 mg/L humic acid). These ranges represent what is commonly found in the environment (Table S2). We also conducted adsorption studies at different temperatures (25–50 °C) to estimate adsorption thermodynamics parameters. See the details of these studies in Sections S3-S5.

2.4. Statistical analyses

We performed statistical analysis using RStudio (RStudio 2022.07.1+544). We checked the dataset for normality using the Shapiro-Wilk test and homogeneity of variance using Levene's test. We accepted data when normality and homogeneity of variance have $p > 0.05$. We evaluated statistical significance for normally distributed data using two-way analysis of variance (ANOVA) and post-hoc Tukey's HSD test. Datasets that did not satisfy homoscedasticity were analyzed using Kruskal-Wallis non-parametric statistical analysis.

3. Results and discussions

3.1. Characterization of secondary PET MPs

Unlike the transparent PET bottles, the produced secondary PET MPs were pale white in color (Fig. 1a). The overall particle size distribution was 39–493 μm, with about 63 % within 50–190 μm (Fig. 1b). The polydispersity index (PDI) was 0.302, suggesting a moderately broad distribution [45]. The size distribution is close to what we intended to produce (53–250 μm), meaning our adopted method can produce secondary PET MPs of desired sizes. We also observed that the surface of the MPs was rough, and they had irregular shapes (Fig. 1c), similar to secondary MPs isolated from the natural environment [46]. The BET surface area of the MPs was 3.82 $m^2/g \pm 0.05$ m^2/g. The BET surface area obtained is larger than what was reported for secondary PET MPs (180–220 μm) produced using a crusher (1.42 $m^2/g \pm 0.03$ m^2/g) [47], aged PET MPs (125 μm; 1.22–1.56 m^2/g) [48], and smaller-sized primary PET MPs (11–28 μm; 0.88 ± 0.01 m^2/g).[49] The observed difference in surface area is likely due to differences in particle size and morphology resulting from the different production methods [50].

The FTIR spectra of the secondary MPs and that of the PET water bottle were similar (Fig. 1d), which shows that the mechanical breakdown approach used in this study did not alter the surface chemistry of the polymer. The peak assignment for the FTIR spectra is shown in Fig. S2. Both spectra match that of standard PET [51]. The ester (-COO-) group, formed from the condensation of terephthalic acid and ethylene glycol, is the main functional group present in PET. The peaks at 1089 and 1712 cm^{-1} were assigned to the stretching vibration of C-O and -C═O bonds, respectively, in the -COO- group. We assigned the peak at 1021 cm^{-1} to the stretching vibrations of the ester (-C-O-C-) group. We also observed symmetry C-H bending of aromatic rings at 2971 cm^{-1}. Although PET may contain some residual hydroxyl (OH) group from ethylene glycol, the OH group is often converted to -COO group [52,53]. Therefore, it is unsurprising that the OH functional group was not observed in the spectrum obtained.

3.2. Kinetics of PFAS adsorption onto secondary PET MPs

In single-analyte solutions, the five PFAS were rapidly adsorbed during the first 30 min and reached equilibrium after 420 min (Fig. S3), which implies that the partitioning of PFAS to the surface of secondary

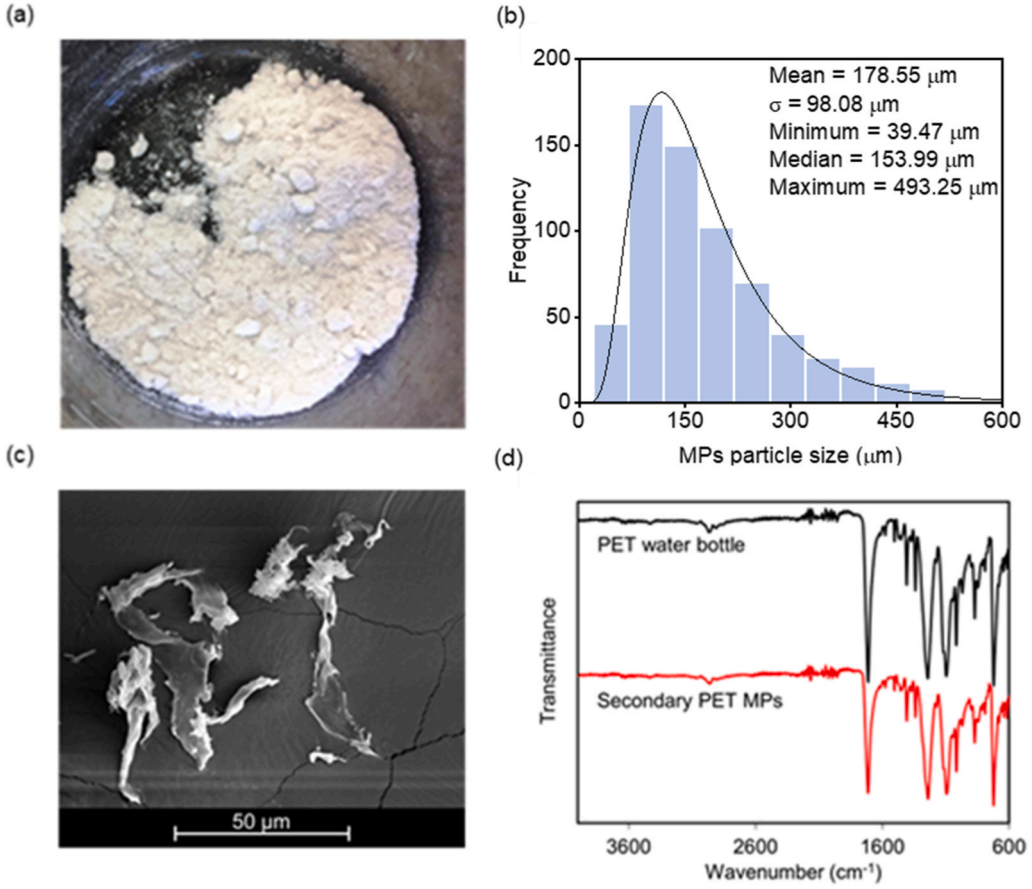

Fig. 1. (a) The appearance, (b) particle size distribution, and (c) SEM micrograph of secondary PET MPs used in this study. (d) A comparison of the FTIR spectra of the secondary PET MPs and the parent PET water bottle. The peak assignment for the FTIR spectra is shown in Fig. S2.

PET MPs in waters likely occurs in the order of hours. The kinetics of PFAS adsorption to the PET MPs was best described by the pseudo-first-order (PFO) model, although the pseudo-second-order (PSO) model was suitable, too (Table S3). The only exception we observed was for GenX, for which the intraparticle diffusion (IPD) and PSO models had the best correlation coefficients (both $R^2 > 0.83$). It is somewhat surprising that the IPD model better describes the adsorption of GenX, given that its relatively large molecular size might limit its diffusion. Moreover, secondary PET MPs are not very porous (pore volume = 0.000947 cm^3/g). The excellent fit of the PFO and PSO models for describing the adsorption kinetics of the PFAS is not surprising, given their hydrophobic backbone (and hence, tendencies for physical interactions) and functional head groups (and thus, the possibility of participating in chemical interactions such as hydrogen bonding, as shown in Table S1).

Based on the PFO adsorption rate constant (k_1) we obtained (Fig. 2a, Table S3) perfluoroalkyl carboxylic acids (PFCAs) adsorbed faster to the secondary PET MPs (k_1 = 0.052 ± 0.027 /min for PFOA and 0.038 ± 0.022 /min for PFBA) compared to perfluoroalkyl sulfonic acids (PFSAs) with similar chain lengths (k_1 = 0.036 ± 0.016 /min for PFOS and 0.022 ± 0.005 /min for PFBS). We hypothesize that the faster adsorption of the PFCAs may have to do with their lower molecular weight (compared to the corresponding PFSAs), which allows for faster diffusion from the bulk to the MPs surface. In addition, smaller molecules experience lesser steric constraints when diffusing into nanoscale pores of the secondary MPs, similar to other adsorbents. Our observation of faster adsorption kinetics for PFCAs agrees with other PFAS adsorption studies conducted with plastic [32], and non-plastic surfaces [54,55]. For instance, Dong et al. [55] attributed their observation of faster adsorption of PFOA (than PFOS) to the relatively smaller PFOA size, which resulted in less steric hindrance during the adsorption.

Contrary to the trend in k_1, we observed that the adsorption capacity of the secondary PET MPs (q_e) was greater for PFSAs (q_e = 36.71 μg/g for PFOS and 35.46 μg/g for PFBS) compared to their corresponding PFCAs (q_e = 18.98 μg/g for PFOA and 5.17 μg/g for PFBA) (Fig. 2b). We hypothesize that the higher affinity of the MPs for the sulfonates may be due to the sulfonates' higher hydrophobicity (see LogD values in Table S1). For example, PFOS has an extra CF_2 group compared to PFOA, which imparts a higher hydrophobicity on PFOS (which is similar for PFBS vs. PFBA) [56]. The overall trend of q_e was PFOS > PFBS > GenX > PFOA > PFBA, which is comparable to our recent observation of PFAS partitioning to plastic containers [32].

Within the same functional group, the q_e of the secondary PET MPs for long-chain PFAS (PFOS and PFOA) was higher than that of their short-chain homologs (PFBS and PFBA). We attributed this to the stronger hydrophobic interactions between the MPs and long-chain PFAS due to their possession of higher numbers of the hydrophobic CF_2 moiety. Also, long chains allow PFAS to adsorb while experiencing much less electrostatic repulsion (between the negatively charged MP and their anionic headgroups) compared to short chains. Although micelle formation can enhance the partitioning of PFAS from water to solid surfaces, and long-chain PFAS have lower CMCs (Table S1) [57,58], we do not believe that hemi-micelles and micelles formation played

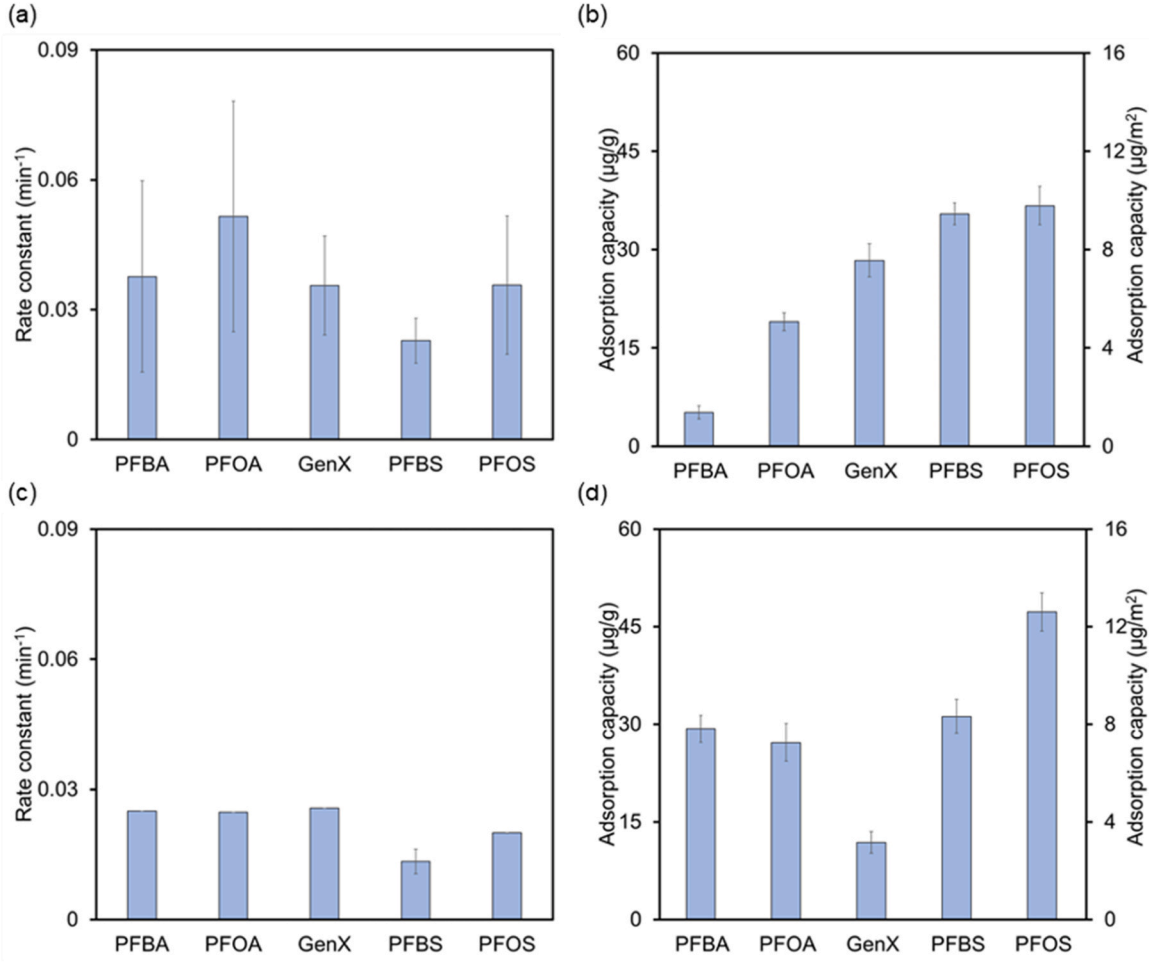

Fig. 2. (a) adsorption kinetics rate constant and (b) capacity of secondary PET MPs for PFAS in single-analyte systems; (c) adsorption kinetics rate constant and (d) capacity of secondary PET MPs for PFAS in mixed-PFAS systems. Initial concentration = 200 μg/L for each PFAS; MPs dose = 2 g/L; pH = 7; shaker speed = 150 rpm. Adsorption kinetics rate constant and capacities were based on the pseudo-first-order (PFO) model.

an important role in this study because the tested concentration (200 μg/L) is 4–5 orders of magnitude below the CMC values of the PFAS we used.

When we studied the adsorption kinetics of a mixture of the five PFAS (200 μg/L each), equilibrium was reached at a longer time (after 540 min) than in the single-PFAS systems (Fig. S4). Similar to the result we obtained in the single-analyte kinetic experiments, PFO and PSO models adequately described the adsorption kinetics of most of the PFAS to the secondary PET MPs. However, the k_1 we obtained for all the PFAS was lower in the mixed-PFAS system than the single-PFAS one (Fig. 2c). This suggests that there was competition among the PFAS for the surface of the secondary PET MPs, which needs to be thoroughly investigated in future studies.

3.3. Effect of water chemistry on adsorption of PFAS onto secondary PET MPs

We initially performed adsorption isotherm experiments in DI water at pH 7 using the equilibrium time determined for the PFAS (Fig. S5). Overall, the Freundlich model fits better with our experimental data (R^2 = 0.87–0.98), which is not surprising given the heterogeneity of the secondary MPs surface (Fig. 1c). The maximum adsorption capacities of the secondary PET MPs for the PFAS (q_{max}) that we determined from the isotherm studies (Table S4) agreed with the q_e values that we independently obtained in the kinetics study (Table S3). To understand how important environmental factors would affect the adsorption of PFAS to secondary MPs in aquatic systems, we performed additional studies, considering the roles of pH, ionic strength, NOM, and temperature.

3.3.1. Role of pH

Like other particles suspended in water, pH may influence the surface charge of MPs [59], which may impact their adsorption of dissolved contaminants. We observed that the q_e of the secondary PET MPs for the five PFAS decreased significantly ($p < 0.05$) as pH increased from 3 to 11 (Fig. 3a, Table S5). Linear regression analyses revealed a statistically significant ($p < 0.05$) inverse correlation between pH and the q_e of the secondary PET MPs for the five PFAS ($-2.18 \geq$ slope ≥ -4.52; $R^2 >$ 0.87), as shown in Fig. S6. We hypothesized that the strong trend between pH and q_e was likely due to the impact of pH on the surface charge of the PET MPs and, thus, electrostatic interactions with the PFAS.

To test this hypothesis, we determined the surface charge of the secondary MPs by measuring their ζ potential at pH 3–11. As expected, the MPs became more negatively charged as pH increased, with ζ potential decreasing in magnitude from − 12.2 mV at pH 3 to − 22.8 mV at pH 11 (Fig. 3b). The change in ζ potential is primarily due to the deprotonation of the secondary PET MP's functional groups, such as carboxylic acids (Fig. 1d), as pH increases. The PFAS considered in this study have $pK_a < 1$ (Table S1) and are therefore anionic at pH 3 – 11. Thus, the magnitude of electrostatic repulsion between the PET MPs and the anionic PFAS increases as water pH increases, limiting the partitioning of PFAS to the surface of the MPs. Our observation agrees with the trend that has been reported by other researchers for the adsorption of PFAS to solids, such as MPs [31,60], soil/sediment [61,62], and nanoparticles [63], at different pH values. In most studies, the trends were attributed to changes on the surface of the adsorbents brought about by pH change.

3.3.2. Role of ionic strength

Overall, we observed that (1) the q_e of the secondary PET MPs for the five PFAS increased as the ionic strength of water increased; and (2) the increase in q_e as ionic strength increased from 0 to 100 mM was statistically significant ($p < 0.05$) for only the short-chain PFAS (Fig. 3c, Table S6). For instance, the q_e for PFBA increased significantly ($p = 0.01$) from 7.6 ± 0.9 μg/g at 0 mM to 23.7 ± 7.6 μg/g at 100 mM, while the q_e for PFOS also increased (but not significantly; $p = 0.11$) from 38.6 ± 4.8 μg/g at 0 mM to 58.2 ± 8.9 μg/g at 100 mM. Based on a regression analysis, q_e is overall not significantly ($p > 0.05$) linearly correlated to ionic strength (Fig. S7), perhaps due to the insignificance of the effect of ionic strength on the q_e for the long-chain PFAS. Increased adsorption of PFAS to the secondary PET MPs as ionic strength increases may arise from the impact of the ions on the surface charge of the adsorbents, and on the solubility of the adsorbates.

We observed increased positivity of the surface charge (based on ζ potential) of the secondary PET MPs with increased ionic strength. The ζ potential of the secondary MPs increased from − 36.7 ± 1.97 mV at 0.1 mM to − 20.5 ± 2.38 mV at 100 mM NaCl (Fig. 3d). The charge screening we observed with increased ionic strength is due to electrical double layer (EDL) compression by Na^+, as predicted by the classical colloidal theory [59,64]. The increased positivity of the MPs' surfaces likely decreased the electrostatic repulsion between MPs and the anionic headgroups of the PFAS, allowing for more adsorption. Increased ionic strength probably favored more adsorption of the short-chain PFAS than the long-chain PFAS because the short-chain PFAS experience electrostatic repulsion much more than their long-chain homologs due to the shorter distance between their hydrophobic tails and anionic headgroups. In addition, increasing ionic strength disrupts the hydration shell around PFAS molecules, making them more likely to interact with surfaces via hydrophobic interactions. This increase in hydrophobic interactions is more pronounced in short-chain PFAS than in the long-chain counterparts, which are inherently more hydrophobic [33].

Increased ionic strength could also enhance the adsorption of PFAS (especially the long chain homologs, which are more hydrophobic) through the salting-out effect (deceased solubility), neutralization of charges on the functional group (which increases hydrophobicity), and micelle/hemi-micelle formation [33,65]. However, the concentration of PFAS used in this study is several orders of magnitude below their solubility and CMC in water (Table S1), and all the PFAS are anionic at the pH studied. Our finding of increased adsorption of PFAS to PET MPs at higher ionic strengths agrees with Wang and coworkers, who reported increased adsorption of PFOS to polyethylene, polystyrene, and polyvinyl chloride when the system's salt concentration increased [31]. It is also important to note that in addition to Na^+, divalent cations (such as Ca^{2+}, Mg^{2+}, etc.) are present in the environment [41,66,67], which may have even stronger effects on PFAS adsorption to MPs [31]. Based on our results, we expect weak adsorption of short-chain PFAS (compared to their longer-chain homologs) to secondary PET MPs in freshwaters, which typically have low salinity. Meanwhile, adsorption of short-chain PFAS will be enhanced in estuaries and marine systems, which have much higher salt content that can screen the surface charge of MPs (colloids).

Generally, the q_e of the secondary MPs was greater for the sulfonates than their analogous carboxylates at every ionic strength tested (Table S6). For instance, the q_e for PFBA increased significantly ($p = 0.01$) from 7.6 ± 0.9 μg/g at 0 mM to 23.7 ± 7.6 μg/g at 100 mM. Similarly, the q_e for PFBS increased significantly ($p = 0.01$) from 32.1 ± 4.2 μg/g at 0 mM to 49.0 ± 7.8 μg/g at 100 mM. We expected a greater influence of ionic strength on the sulfonates (than the carboxylates) because the sulfonate functional group has a higher negative charge than the carboxylate functional group [32,33], which should result in a stronger electrostatic attraction with the secondary MP surface (as they become less negatively charged with increasing ionic strength). Considering the correlation analysis we performed (Fig. S7), the slope of the regression line for PFOS (0.1198 mMg/μg) was greater than that for PFOA (0.1079 mMg/μg). However, the slope of the regression line for PFBS (0.0924 mMg/μg) was less than PFBA's (0.1069 mMg/μg). As such, our results do not support the hypothesis that ionic strength consistently has a higher impact on sulfonate adsorption compared to carboxylates. Our study may have multiple interplays of functional group and chain length. Considering more compounds in the PFSA and PFCA groups will likely reveal a clearer trend.

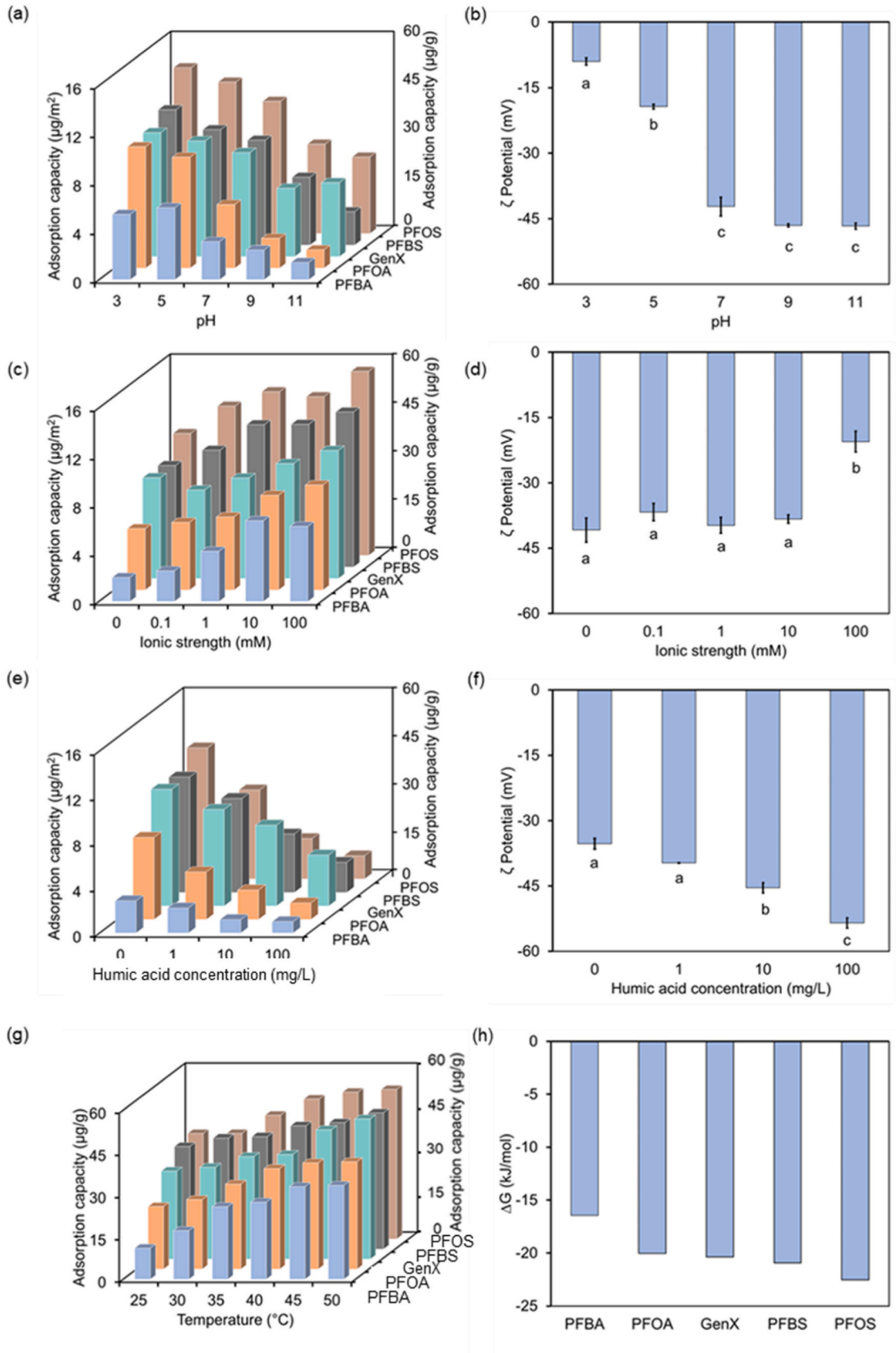

Fig. 3. Effect of pH on (a) the adsorption capacity and (b) ζ potential of PET MPs. Effect of ionic strength on (c) the adsorption capacity and (d) ζ potential of PET MPs. Effect of humic acid concentration on (e) the adsorption capacity and (f) ζ potential of PET MPs. Effect of temperature on (g) the adsorption capacity of PET MPs. Gibb's free energy (ΔG) of adsorption at 25 °C is shown in (h). Initial PFAS concentration = 200 μg/L; MPs dose = 2 g/L; shaker speed = 150 rpm.

3.3.3. Effect of NOM

Humic acid (0–100 mg/L) was used as a surrogate for NOM, which is abundant in aquatic environments [41,68]. Although the humic acid used here is orders of magnitude higher in concentration than the PFAS, it represents what is expected in natural and engineered aquatic systems [68]. We found that the adsorption of all five PFAS to the secondary PET MPs decreased significantly ($p < 0.05$) as humic acid concentration increased (Fig. 3e, Table S7). However, there was no statistically significant linear correlation between q_e and humic acid concentration (Fig. S8). Within the same functional groups, humic acid had a higher impact on the long-chain PFAS than the short-chain homologs. For instance, while the q_e for PFBA and PFBS decreased by 64.9 % and 73.8 %, respectively, when humic acid increased from 0 to 100 mg/L, the decrease in the q_e for PFOA and PFOS was 79.9 % and 82.3 %, respectively. The results suggest that humic acid competes with PFAS for adsorption on the surface of the MPs. While the general trend of the impact of NOM would be similar, the molecular-scale mechanism of effect may be somewhat different, depending on the NOM fraction used as a surrogate (e.g., fulvic acid or humic acid).

The hydrophobic regions of humic acid molecules can bind to MPs surfaces, limiting access for PFAS via steric repulsion. With increasing humic acid concentrations, more sorption sites of the MPs become occupied. Adsorbed PFAS can also be displaced by more hydrophobic organic matter [69]. Due to its possession of charged moieties, humic acid can also alter the surface charge of colloids [59,67,70]. We measured the ζ potential of the secondary PET MPs in the presence of humic acid and observed an increase in the negativity of the surface charge of the MPs (ζ potential decreased from −35.3 mV to −53.5 mV as humic acid concentration in aqueous media increased from 0 to 100 mg/L (Fig. 3f). Therefore, in addition to steric exclusion of PFAS from the surface of the MPs, humic acid increased the electrostatic repulsion between the humic acid-coated MPs and PFAS. While Mejías *et al.* similarly found a negative effect of humic acid on the adsorption of PFAS to polyamide MPs [71], Ateia and coworkers found that NOM generally promoted the adsorption of long-chain PFAS onto MPs and had no adverse effect on GenX [27]. The major difference between our experimental setup and that of Ateia *et al.* is that they mixed their MPs in NOM-containing water for 14 d (which preloads the NOM on the MPs) before studying the adsorption of PFAS. Thus, it is likely that the interactions among MPs, NOM, and PFAS change over time, with competition (between NOM and PFAS) being the dominant process when MPs initially enter a water body, while co-sorption becomes more dominant over time as NOM adsorption reaches equilibrium.

3.3.4. Role of temperature

As we increased the temperature of the reactor from 25 to 50 °C, the q_e of the secondary PET MPs for the PFAS increased significantly ($p < 0.05$), except for PFOS, for which the increase was not statistically significant ($p > 0.05$) (Fig. 3g; Table S9). Linear regression analyses revealed a statistically significant ($p < 0.05$) direct correlation between temperature and the q_e of the PET MPs for the five PFAS ($0.91 \geq \text{slope} \geq 0.45$; $R^2 > 0.92$), as shown in Fig. S9. Increased q_e at elevated temperatures suggests a more favorable interaction between PFAS and the secondary PET MPs. This may have originated from (1) increased collision between the adsorbate and adsorbent due to elevated kinetic energy as the temperature of the endothermic reaction system increased, (2) more collision occurring in the right orientation in space due to increased PFAS diffusion, and (3) increase in the fraction of collisions with enough energy for adsorption, based on the Collision Theory. Although we were unable to verify it in this work, Khumalo *et al.* hypothesized that plastic pore-filling could be an important mechanism of PFAS partitioning, especially at high temperatures due to polymer (pore) expansion [72].

Based on the Gibb's free energy (ΔG) we obtained at 25 °C (Fig. 3h), which ranged from − 16.4 kJ/mol (for PFBA) to − 22.5 kJ/mol (for PFOS), we concluded that the adsorption of the five PFAS to the secondary PET MPs is thermodynamically spontaneous at ambient condition and would occur in the environment. Also, the ΔG of the adsorption of PFAS to the secondary PET MPs became more negative as temperature increased (Table S9), which is reasonable given that it is an endothermic process ($\Delta H = 14.0$ to 41.0 kJ/mol). Based on the increase in free energy spontaneity at higher temperatures, and the relatively low enthalpy values, we also concluded that the adsorption of the PFAS to the secondary PET MPs is mainly via physical interactions [40]. The spontaneity of PFAS adsorption to the MPs was caused primarily by increased randomness, as indicated by positive entropy (ΔS) [73]. While this is the first study to determine the thermodynamic spontaneity of PFAS adsorption to MPs experimentally, other researchers reported spontaneous adsorption of PFOS to humic acid [74], polyaniline nanotubes [75], and carbon nitrides [76].

3.4. Mechanism of adsorption

To better understand the mechanism of interactions between the secondary PET MPs and PFAS, we collected the FTIR spectra of the MPs before and after PFAS adsorption to assess any changes in surface functionality after adsorption. The obtained spectra (Fig. 4a) were transformed (second derivative) and compared using principal component analysis (PCA), to separate overlapping bands and magnify any minor spectral variations [23,32]. PCA revealed clear separations between the spectra collected before and after PFAS adsorption, except for PFBA. The separations we observed after PFAS adsorption indicate changes in the infrared spectra of the MPs after adsorption, and it is reasonable that the changes in the MPs spectra after PFBA adsorption were not substantial given that the q_e for PFBA (5.17 ± 0.99 μg/g) is a factor 4 (or more) lower than the other PFAS (18.98 ± 1.37 - 36.71 ± 2.94 μg/g).

We determined the bands (wavenumbers) with the highest square loadings, which represent altered features (wavenumbers) that are mainly responsible for the observed separations along the PCs [77]. This check reveals a consistent decrease in the intensity of peaks assigned to the stretching vibration of C-O (at 1089 cm^{-1}) and -C═O (at 1712 cm^{-1}) bonds in the ester (-COO-) group of the secondary PET MPs after PFAS adsorption. We attributed the decrease in the intensities of these peaks to hydrophobic interactions between the MPs and PFAS, in which PFAS displaced the water molecules adsorbed to the surface of the PET MPs [78,79]. The displacement of adsorbed water and, thus, the breaking of some hydrogen bonds water molecules formed with secondary PET's -COO- group changed the chemical environment around these groups and decreased their intensity after PFAS adsorption. We calculated the change in the intensity of secondary PET's -COO- group after the adsorption of each PFAS (Table S10) and found a strong, significant correlation ($R^2 = 0.96$; $p = 0.003$) between it and ΔS (Fig. S10). This suggests that the increase in randomness after adsorption may be due to displacement of water by the PFAS [80,81].

We further investigated the adsorption mechanism of PFAS to the secondary PET MPs using DFT. Molecular descriptors obtained from DFT improve understanding of the nature of reactions at the molecular levels. Details of the computational method adopted are provided in Section S6. Frontier orbital analysis of the optimized PET and PFAS structures shows interaction sites where the highest occupied molecular orbitals (HOMO) and lowest unoccupied molecular orbitals (LUMO) are localized on each molecule (Fig. 5). According to frontier molecular orbital theory, the effectiveness of the interaction between two reacting molecules is linked to their frontier orbital distributions and the energy gaps maintained within. The HOMO-LUMO orbitals of the PFSAs are spread out from the sulfonate head to the C-F tail, while those of the PFCAs are localized on the carboxylate head and nearby fluorine atoms.

Considering that the spread in the HOMO-LUMO of any molecule influences its dipole moment and, hence, likely interactions with solid surfaces, we explored the role of PFAS polarity on their adsorption to the secondary PET MPs. The solid-water partitioning coefficients (K_d) of the

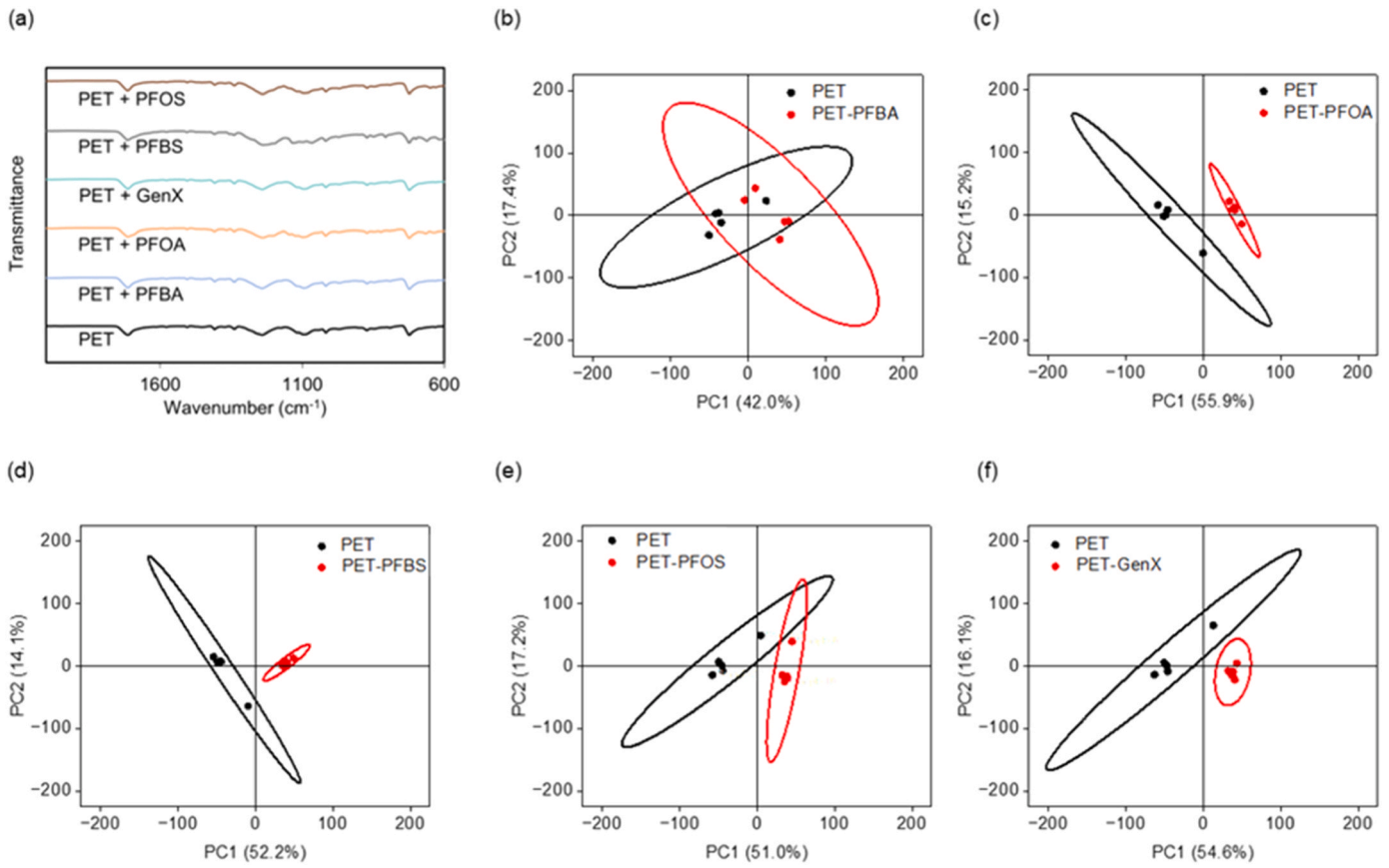

Fig. 4. (a) FTIR spectra of the secondary PET MPs before and after PFAS adsorption. PCA score plot of transformed FTIR spectra of PET before and after adsorption of (b) PFBA, (c) PFOA, (d) PFBS, (e) PFOS, and (f) GenX. The ellipses in the PCA score plots represent the 95 % confidence range; n = 5 for each treatment.

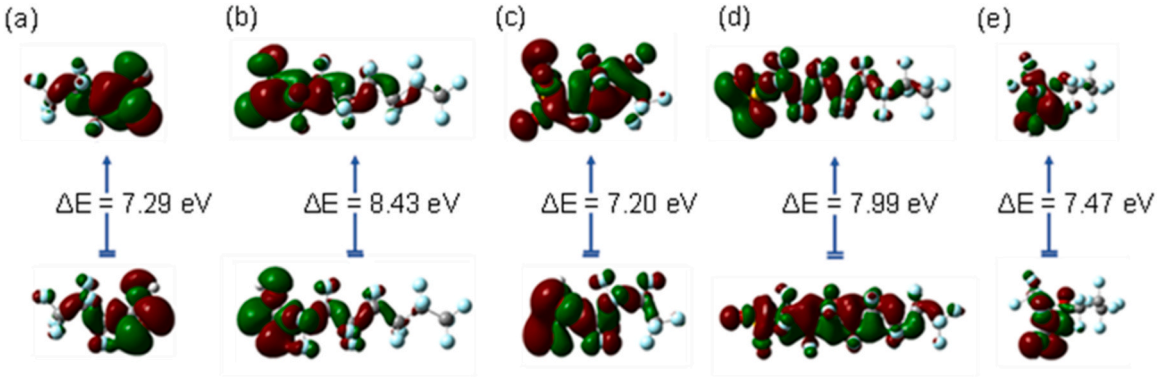

Fig. 5. HOMO-LUMO diagrams of (a) PFBA, (b) PFOA, (c) PFBS, and (d) PFOS (e) GenX.

secondary PET MPs for the PFAS in our experiments had a significant correlation ($R^2 = 0.89$; $p = 0.015$) with the theoretical dipole moment obtained from DFT calculations (Table S11; Fig. S11). This further confirms that electrostatic interactions are very important in the adsorption of PFAS to the secondary PET MPs. The active sites of the PFCAs are centered on the two oxygen atoms on the carboxylic head, with both oxygen atoms having the highest f_k^+ and f_k^- values (Tables S12-13). Similarly, the three oxygen atoms double-bonded to the central sulfur atom in the sulfonic head group of the PFSAs have the highest f_k^+ and f_k^- values. These centers represent sites most prone to nucleophilic and electrophilic interactions, and likely interact electrostatically with the secondary PET MPs. PFOS has the smallest HOMO-LUMO gap, indicating greater polarizability. Its electron cloud can be distorted to induce interactions with a charged surface. The additional fluorine atoms in PFOS (compared to other PFAS considered in this study) further lower its HOMO energy and increase its partial positive charge for electrostatic attraction to a negatively charged surface like secondary PET MPs.

4. Conclusion

We produced secondary PET MPs (39 – 493 μm) by blending PET water bottles. We evaluated their affinity for five common PFAS, which are PFBA, PFBS, PFOA, PFOS, and GenX, under different water chemistry conditions. The capacity of the secondary PET MPs for the five PFAS increased as ionic strength or temperature was increased and decreased as pH or NOM concentration was increased. We found that the adsorption of PFAS to the surface of secondary PET MPs is

thermodynamically spontaneous at 25 °C, and it occurs in the order of hours. This implies that PFAS will spontaneously adsorb onto the surface of secondary PET MPs in natural and engineered aquatic systems. Based on the results, we expect more adsorption of PFAS to secondary PET MPs in seawater, which typically has a high ionic strength and lower NOM concentration, relative to freshwater. The adsorption of PFAS to secondary PET MPs will be dynamic in estuary systems due to salinity gradient, with K_d increasing as water flows from freshwater seaward.

We studied secondary microplastics generated from PET water bottles as a representative of this diverse MPs category. We acknowledge that secondary MPs encompass various polymer types and degradation mechanisms, making them complex. While we focused on mechanically degraded PET MPs, there is a need for further research to explore the adsorption behavior of different polymer types and degradation stages. In addition, we employed humic acid as a representative component of NOM and studied the effect of ionic strength by varying Na^+ concentration. NOM also comprises other important fractions, and natural waters contain Ca^{2+}, Mg^{2+}, etc. To increase the fundamental understanding of PFAS-MPs at the molecular scale, it is necessary to consider different components of NOM and other ions in water.

The partitioning of PFAS onto MPs in aquatic systems implies that organisms are likely exposed to higher doses of PFAS than are present in water if they ingest PFAS-adsorbed MPs. This is common in waters receiving (treated) wastewater. Therefore, risk assessment of PFAS in aquatic systems should consider their partitioning to MPs and other suspended solids in water. While the importance of partitioning increases as the salinity of water increases and NOM concentration decreases, we note that agglomeration of MPs (which typically decreases surface area/adsorption sites) will be important in saline waters (due to EDL compression, similar to engineered nanomaterials) [41,67]. The adsorption of PFAS to MPs could also affect the colloidal stability and, thus, the fate and transport of the particles in water [82]. Therefore, the potential adsorption of PFAS and other dissolved contaminants should be considered in the risk assessment of MPs.

Environmental Implication

Microplastics (MPs) are abundant in natural and engineered aquatic systems. They have been reported to cause adverse effects to organisms. Similarly, PFAS are ubiquitous in the environment and are potentially toxic. In this study, we investigated interactions between both classes of hazardous materials using commonly detected representatives. Attractive interactions can lead to elevated exposure of organisms to PFAS if they ingest MPs. Despite being an endothermic process, the adsorption of the studied PFAS to MPs is thermodynamically favorable at ambient conditions due to increased entropy (randomness). It also occurs fast, which makes it environmentally relevant.

CRediT authorship contribution statement

Adeyemi S. Adeleye: Writing – review & editing, Writing – original draft, Visualization, Validation, Supervision, Resources, Project administration, Methodology, Investigation, Funding acquisition, Formal analysis, Data curation, Conceptualization. **Christopher I. Olivares:** Resources, Methodology. **Omobayo A. Salawu:** Writing – review & editing, Writing – original draft, Visualization, Validation, Methodology, Investigation, Formal analysis, Data curation, Conceptualization.

Declaration of Competing Interest

The authors declare that they have no known competing financial interests or personal relationships that could have appeared to influence the work reported in this paper.

Data availability

Data will be made available on request.

Acknowledgment

The authors are grateful for support from Brown and Caldwell through the UCI Water-Energy Nexus Center. We also appreciate Lauren Nicole O'Brien, Natasha Thandi, Sarah Kadiri, Hugo Yao, Zachary William Wharton, and Ivan Doan for their help with microplastics preparation. The FTIR analysis was performed at UCI Laser Spectroscopy Labs, while SEM was done at the UC Irvine Materials Research Institute (IMRI). IMRI is partly supported by the National Science Foundation through the UC Irvine Materials Research Science and Engineering Center (DMR-2011967).

Appendix A. Supporting information

Supplementary data associated with this article can be found in the online version at doi:10.1016/j.jhazmat.2024.134185.

References

[1] Geyer, R., Jambeck, J.R., Law, K.L., 2017. Production, use, and fate of all plastics ever made. Sci Adv 3 (7), e1700782.
[2] Wang, F., et al., 2020. Sorption behavior and mechanisms of organic contaminants to nano and microplastics. Molecules 25 (8), 1827.
[3] Elias, SA, Plastics in the Ocean, in Encyclopedia of the Anthropocene, D.A. Dellasala and M.I. Goldstein, Editors; 2018, Elsevier: Oxford. p. 133–149.
[4] Europe, P.J.P., 2022. Plastics– facts 2022 1, 1–81.
[5] Elhacham, E., et al., 2020. Global human-made mass exceeds all living biomass. Nature 588 (7838), 442–444.
[6] Jambeck, J.R., et al., 2015. Plastic waste inputs from land into the ocean. Science 347 (6223), 768–771.
[7] Cheng, Y., et al., 2021. Occurrence and abundance of poly- and perfluoroalkyl substances (PFASs) on microplastics (MPs) in Pearl River Estuary (PRE) region: Spatial and temporal variations. Environ Pollut 281, 117025.
[8] da Costa, J.P., et al., 2016. Nano)plastics in the environment – sources, fates and effects. Sci Total Environ 566-567, 15–26.
[9] Zhang, K., et al., 2021. Understanding plastic degradation and microplastic formation in the environment: a review. Environ Pollut 274, 116554.
[10] Corcoran, PL, Degradation of Microplastics in the Environment, in Handbook of Microplastics in the Environment, T. Rocha-Santos, M. Costa, and C. Mouneyrac, Editors; 2020, Springer International Publishing: Cham. p. 1–12.
[11] Ter Halle, A., et al., 2017. Nanoplastic in the North Atlantic subtropical gyre. Environ Sci Technol 51 (23), 13689–13697.
[12] Alimi, O.S., et al., 2018. Microplastics and nanoplastics in aquatic environments: aggregation, deposition, and enhanced contaminant transport. Environ Sci Technol 52 (4), 1704–1724.
[13] Barnes, D.K.A., et al., 2009. Accumulation and fragmentation of plastic debris in global environments. Philos Trans R Soc B: Biol Sci 364 (1526), 1985–1998.
[14] Shim, W.J., Hong, S.H., Eo, S., 2018. Chapter 1 - marine microplastics: abundance, distribution, and composition. In: Zeng, E.Y. (Ed.), Microplastic contamination in aquatic environments. Elsevier, pp. 1–26.
15 Petroody, S.S.A., Hashemi, S.H., van Gestel, C.A.M., 2020. Factors affecting microplastic retention and emission by a wastewater treatment plant on the southern coast of Caspian Sea. Chemosphere 261, 128179.
[16] Rochman, C.M., et al., 2015. Anthropogenic debris in seafood: Plastic debris and fibers from textiles in fish and bivalves sold for human consumption. Sci Rep 5 (1), 1–10.
[17] Ziajahromi, S., et al., 2017. Wastewater treatment plants as a pathway for microplastics: development of a new approach to sample wastewater-based microplastics. Water Res 112, 93–99.
[18] Koelmans, A.A., et al., 2016. Microplastic as a Vector for Chemicals in the Aquatic Environment: Critical Review and Model-Supported Reinterpretation of Empirical Studies. Environ Sci Technol 50 (7), 3315–3326.
[19] Yu, F., et al., 2019. Adsorption behavior of organic pollutants and metals on micro/nanoplastics in the aquatic environment. Sci Total Environ 694, 133643.
[20] Han, Z., et al., 2023. Perfluorooctanoic acid dominates the molecular-level effects of a trace mixture of perfluorooctanoic acid and perfluorooctane sulfonic acid in earthworm. ChemRxiv.
[21] Brusseau, M.L., Anderson, R.H., Guo, B., 2020. PFAS concentrations in soils: background levels versus contaminated sites. Sci Total Environ 740, 140017.
[22] Buck, R.C., et al., 2011. Perfluoroalkyl and polyfluoroalkyl substances in the environment: Terminology, classification, and origins. Integr Environ Assess Manag 7 (4), 513–541.
[23] Han, Z., et al., 2023. Perfluorooctanoic acid dominates the molecular-level effects of a mixture of equal masses of perfluorooctanoic acid and perfluorooctane sulfonic acid in earthworm. J Hazard Mater 457, 131718.

[24] Navarathna, C.M., et al., 2023. Microplastics and per- and polyfluoroalkyl substances (PFAS) analysis in sea turtles and bottlenose dolphins along mississippi's coast. Analytica 4 (1), 12–26.
[25] Allouzi, M.M.A., et al., 2021. Micro (nano) plastic pollution: The ecological influence on soil-plant system and human health. Sci Total Environ 788, 147815.
[26] Song, Y.K., et al., 2017. Combined effects of UV exposure duration and mechanical abrasion on microplastic fragmentation by polymer type. Environ Sci Technol 51 (8), 4368–4376.
[27] Ateia, M., et al., 2020. Sorption behavior of real microplastics (MPs): Insights for organic micropollutants adsorption on a large set of well-characterized MPs. Sci Total Environ 720, 137634.
[28] Cole, M., et al., 2011. Microplastics as contaminants in the marine environment: a review. Mar Pollut Bull 62 (12), 2588–2597.
[29] Bhagat, K., et al., 2022. Aging of microplastics increases their adsorption affinity towards organic contaminants. Chemosphere 298, 134238.
[30] Waldman, W.R., Rillig, M.C., 2020. Microplastic research should embrace the complexity of secondary particles. ACS Publ.
[31] Wang, F., Shih, K.M., Li, X.Y., 2015. The partition behavior of perfluorooctanesulfonate (PFOS) and perfluorooctanesulfonamide (FOSA) on microplastics. Chemosphere 119, 841–847.
[32] Zenobio, J.E., et al., 2022. Adsorption of per- and polyfluoroalkyl substances (PFAS) to containers. J Hazard Mater Adv 7, 100130.
[33] Llorca, M., et al., 2018. Adsorption of perfluoroalkyl substances on microplastics under environmental conditions. Environ Pollut 235, 680–691.
[34] Kershaw, P, Marine plastic debris and microplastics–Global lessons and research to inspire action and guide policy change; 2016: United Nations Environment Programme.
[35] Ji, Y., et al., 2020. Realistic polyethylene terephthalate nanoplastics and the size- and surface coating-dependent toxicological impacts on zebrafish embryos. Environ Sci: Nano 7 (8), 2313–2324.
[36] Guo, X., et al., 2022. The distinct toxicity effects between commercial and realistic polystyrene microplastics on microbiome and histopathology of gut in zebrafish. J Hazard Mater 434, 128874.
[37] Uurasjärvi, E., et al., 2020. Microplastic concentrations, size distribution, and polymer types in the surface waters of a northern European lake. Water Environ Res 92 (1), 149–156.
[38] Kameda, Y., Yamada, N., Fujita, E., 2021. Source-and polymer-specific size distributions of fine microplastics in surface water in an urban river. Environ Pollut 284, 117516.
[39] Xu, X., et al., 2019. Microplastics in the wastewater treatment plants (WWTPs): occurrence and removal. Chemosphere 235, 1089–1096.
[40] Salawu, O.A., Han, Z., Adeleye, A.S., 2022. Shrimp waste-derived porous carbon adsorbent: performance, mechanism, and application of machine learning. J Hazard Mater, 129266.
[41] Adeleye, A.S., et al., 2019. Fate and Transformation of Graphene Oxide in Estuarine and Marine Waters. Environ Sci Technol 53 (10), 5858–5867.
[42] Kurwadkar, S., et al., 2022. Per- and polyfluoroalkyl substances in water and wastewater: a critical review of their global occurrence and distribution. Sci Total Environ 809, 151003.
43 Phong Vo, H.N., et al., 2020. Poly-and perfluoroalkyl substances in water and wastewater: a comprehensive review from sources to remediation. J Water Process Eng 36, 101393.
[44] ASTM, 2020. Standard practice for determination of adsorptive capacity of activated carbon by aqueous phase isotherm technique. ASTM International, West Conshohocken, PA.
[45] Danaei, M., et al., 2018. Impact of particle size and polydispersity index on the clinical applications of lipidic nanocarrier systems. Pharmaceutics 10 (2), 57.
[46] Malygina, N., et al., 2021. Microplastic Pollution in the Surface Waters from Plain and Mountainous Lakes in Siberia, Russia. Water 13 (16), 2287.
[47] Duan, L., et al., 2023. Sulfide-and UV-induced aging differentially affect contaminant-binding properties of microplastics derived from commercial plastic products. Sci Total Environ 869, 161800.
[48] Hanun, J.N., et al., 2023. Weathering effect triggers the sorption enhancement of microplastics against oxybenzone. Environ Technol Innov, 103112.
[49] Zhao, M., et al., 2021. Sulfide induces physical damages and chemical transformation of microplastics via radical oxidation and sulfide addition. Water Res 197, 117100.
[50] Costigan, E., et al., 2022. Adsorption of organic pollutants by microplastics: Overview of a dissonant literature. J Hazard Mater Adv 6, 100091.
[51] Jiang, Z., et al., 2019. Preparation and properties of bottle-recycled polyethylene terephthalate (PET) filaments. Text Res J 89 (7), 1207–1214.
[52] Javed, S., Fisse, J., Vogt, D., 2023. Optimization and kinetic evaluation for glycolytic depolymerization of post-consumer PET waste with sodium methoxide. Polymers 15 (3), 687.
[53] Alidadykhah, M., et al., 2022. Functionalization and modification of polyethylene terephthalate polymer by AgCl nanoparticles under ultrasound irradiation as bactericidal. ACS Omega 7 (23), 19141–19151.
[54] Deng, S., et al., 2013. Adsorption of perfluorinated compounds on aminated rice husk prepared by atom transfer radical polymerization. Chemosphere 91 (2), 124–130.
[55] Dong, Q., et al., 2021. Efficient sorption of perfluoroalkyl acids by ionic liquid-modified natural clay. Chem Eng J Adv 7, 100135.
[56] Siriwardena, D.P., et al., 2019. Influence of groundwater conditions and co-contaminants on sorption of perfluoroalkyl compounds on granular activated carbon. Remediat J 29 (3), 5–15.
[57] Yu, Q., et al., 2009. Sorption of perfluorooctane sulfonate and perfluorooctanoate on activated carbons and resin: Kinetic and isotherm study. Water Res 43 (4), 1150–1158.
[58] Du, Z., et al., 2014. Adsorption behavior and mechanism of perfluorinated compounds on various adsorbents—a review. J Hazard Mater 274, 443–454.
[59] Wang, H., et al., 2015. Heteroaggregation of nanoparticles with biocolloids and geocolloids. Adv Colloid Interface Sci 226 (Pt A)), 24–36.
[60] Meng, L., et al., 2023. Influence of microplastics on the photodegradation of perfluorooctane sulfonamide (FOSA). J Environ Sci 127, 791–798.
[61] You, C., Jia, C., Pan, G., 2010. Effect of salinity and sediment characteristics on the sorption and desorption of perfluorooctane sulfonate at sediment-water interface. Environ Pollut 158 (5), 1343–1347.
[62] Nguyen, T.M.H., et al., 2020. Influences of chemical properties, soil properties, and solution pH on soil–water partitioning coefficients of per-and polyfluoroalkyl substances (PFASs). Environ Sci Technol 54 (24), 15883–15892.
[63] Deng, S., et al., 2012. Sorption mechanisms of perfluorinated compounds on carbon nanotubes. Environ Pollut 168, 138–144.
[64] Elimelech, M, et al., Particle Deposition and Aggregation; 1998, Oxford, UK: Butterworth-Heinemann.
[65] Fu, L., et al., 2021. Adsorption behavior of organic pollutants on microplastics. Ecotoxicol Environ Saf 217, 112207.
[66] Salawu, O.A., Han, Z., Adeleye, A.S., 2022. Shrimp waste-derived porous carbon adsorbent: Performance, mechanism, and application of machine learning. J Hazard Mater 437, 129266.
[67] Adeleye, A.S., Keller, A.A., 2014. Long-term colloidal stability and metal leaching of single wall carbon nanotubes: effect of temperature and extracellular polymeric substances. Water Res 49 (0)), 236–250.
[68] Keller, A.A., et al., 2010. Stability and aggregation of metal oxide nanoparticles in natural aqueous matrices. Environ Sci Technol 44 (6), 1962–1967.
[69] Park, M., et al., 2020. Adsorption of perfluoroalkyl substances (PFAS) in groundwater by granular activated carbons: Roles of hydrophobicity of PFAS and carbon characteristics. Water Res 170, 115364.
[70] Adeleye, A.S., Keller, A.A., 2016. Interactions between algal extracellular polymeric substances and commercial tio2 nanoparticles in aqueous media. Environ Sci Technol 50 (22), 12258–12265.
[71] Mejías, C., et al., 2023. Adsorption of perfluoroalkyl substances on polyamide microplastics: Effect of sorbent and influence of environmental factors. Environ Res 216, 114834.
[72] Khumalo, S.M., et al., 2022. Sorption of perfluorinated and pharmaceutical compounds in plastics: a molecular simulation study. Water 14 (12), 1951.
[73] Wang, T., et al., 2020. Adsorption behavior and mechanism of five pesticides on microplastics from agricultural polyethylene films. Chemosphere 244, 125491.
[74] Jia, C., You, C., Pan, G., 2010. Effect of temperature on the sorption and desorption of perfluorooctane sulfonate on humic acid. J Environ Sci 22 (3), 355–361.
[75] Xu, C., Chen, H., Jiang, F., 2015. Adsorption of perflourooctane sulfonate (PFOS) and perfluorooctanoate (PFOA) on polyaniline nanotubes. Colloids Surf A: Physicochem Eng Asp 479, 60–67.
[76] Yan, T., et al., 2014. Adsorption of perfluorooctane sulfonate and perfluorooctanoic acid on magnetic mesoporous carbon nitride. J Chem Eng Data 59 (2), 508–515.
[77] Abdi, H., Williams, L.J., 2010. Principal component analysis. WIREs Comput Stat 2 (4), 433–459.
[78] Zhu, X., et al., 2022. Enhanced adsorption of bromoform onto microplastic polyethylene terephthalate exposed to ozonation and chlorination. Molecules 28 (1), 259.
[79] Guo, X., et al., 2018. Sorption properties of tylosin on four different microplastics. Chemosphere 209, 240–245.
[80] Mashkoor, F., et al., 2018. Exploring the reusability of synthetically contaminated wastewater containing crystal violet dye using Tectona grandis sawdust as a very low-cost adsorbent. Sci Rep 8 (1), 8314.
[81] Warrick, A.W., Solute and contaminant transport, in soil water dynamics. Oxford University Press.
[82] Bere, K., et al., 2023. Microplastics as an adsorption and transport medium for per- and polyfluoroalkyl substances in aquatic systems: Polystyrene and undecafluorohexanoic acid interactions. J Mol Liq 384, 122285.